

Long non-coding RNA CASC11 interacts with YBX1 to promote prostate cancer progression by suppressing the p53 pathway

XIANCHAO SUN^{1*}, SHIYONG XIN^{1*}, YING ZHANG², LIANG JIN¹, XIANG LIU¹,
JIAXIN ZHANG¹, WANGLI MEI¹, BIHUI ZHANG¹, WEIGUO MA³ and LIN YE¹

¹Department of Urology, Shanghai East Hospital, School of Medicine, Tongji University, Shanghai 200120;

²Department of Urology, The Second Affiliated Hospital of Anhui Medical University, Hefei, Anhui 230032;

³Department of Urology, Tongxin People's Hospital, Tongxin, Ningxia 751300, P.R. China

Received April 1, 2022; Accepted June 16, 2022

DOI: 10.3892/ijo.2022.5400

Abstract. Prostate cancer (PCa) is one of the principal causes of cancer-related death worldwide. The roles and mechanisms of long non-coding RNA (lncRNA) involved in the development of PCa remain incompletely understood. The present study aimed to investigate the role and mechanism of lncRNA in PCa tumorigenesis. In the present study, lncRNA cancer susceptibility candidate 11 (CASC11) was revealed to be a crucial regulator of PCa progression. The expression profiles of CASC11 in PCa were identified through analysis of The Cancer Genome Atlas and Gene Expression Omnibus datasets, and validated in human PCa specimens and cell lines. Gain- and loss-of-function assays were utilized to explore the biological role of CASC11 in PCa initiation and progression. RNA-sequencing, RNA pull-down and RNA immunoprecipitation analyses were used to explore potential mechanisms with which CASC11 may be associated. Rescue experiments were further conducted to confirm this association. The present

results revealed that CASC11 was dominantly distributed in the nuclei of PCa cells, and was highly expressed in PCa tissues and cells. Overexpression of CASC11 was markedly associated with increased tumor proliferation and migratory ability. Functionally, decreased proliferation and migration, as well as inhibited xenograft tumor growth, were observed in CASC11-silenced PCa cells, whereas the opposite effects were detected in CASC11-overexpressing cells. Mechanistically, CASC11 promoted progression of the cell cycle and competitively interacted with Y-box binding protein 1 (YBX1) to block the p53 pathway. Given this, poly (β -amino ester) (PBAE)/small interfering RNA-CASC11 (si-CASC11) nanoparticles were applied to inhibit CASC11 expression and enhance the antitumor effect *in vivo*. The results revealed that PBAE/si-CASC11 nanoparticles augmented the antitumor efficacy of CASC11 knockdown *in vivo*. In conclusion, the present study suggested that CASC11 may regulate PCa progression and elucidated a novel CASC11/YBX1/p53 signaling axis, providing a potential lncRNA-directed therapeutic strategy particularly for the treatment of patients with PCa.

Correspondence to: Dr Lin Ye, Department of Urology, Shanghai East Hospital, School of Medicine, Tongji University, 150 Jimo Road, Pudong New District, Shanghai 200120, P.R. China
E-mail: ericyelin@tongji.edu.cn

Dr Weiguo Ma, Department of Urology, Tongxin People's Hospital, 1 Xueyuan Road, Tongxin, Ningxia 751300, P.R. China
E-mail: maweiguo_87@126.com

*Contributed equally

Abbreviations: PCa, prostate cancer; lncRNA, long non-coding RNA; TCGA, The Cancer Genome Atlas; GEO, Gene Expression Omnibus; CASC11, cancer susceptibility candidate 11; RIP, RNA immunoprecipitation; FISH, fluorescence *in situ* hybridization; shRNA, short hairpin RNA; NC, negative control; PBAE, poly (β -amino ester); siRNA, small interfering RNA; EdU, 5-ethynyl-2'-deoxyuridine; PBS, phosphate-buffered saline; IHC, immunohistochemistry; H&E, hematoxylin and eosin

Key words: prostate cancer, CASC11, Y-box binding protein 1, p53 pathway, progression

Introduction

Prostate cancer (PCa) is the most common malignant tumor of the male genitourinary system and it is characterized by a high recurrence rate (1,2). Despite novel technologies and diagnostic methods applied in clinical practice, a large percentage of patients have no obvious symptoms or present with an advanced stage at the time of diagnosis (3). In particular, the incidence of PCa in the Asia-Pacific region is increasing (4). Therefore, precise treatment strategies for PCa and the underlying mechanisms of tumor initiation need to be urgently addressed.

Long non-coding RNAs (lncRNAs) are a specific form of RNA that consist of a transcript >200 nucleotides in length that does not code for protein (5). The mechanisms associated with the effects of lncRNAs on malignant processes in tumors have been reported extensively and some lncRNAs have been demonstrated to serve a critical role in the functionality of pathways associated with PCa. For example, lncRNA PCAT6 has been shown to promote bone metastasis in PCa by interacting with IGF2BP2 to stabilize IGF1R (6). Furthermore,

lncRNA SNHG17 can aggravate PCa progression in a SNORA71B-dependent manner (7). lncRNA NXTAR has been reported to serve as a tumor suppressor that down-regulates AR/AR-V7 expression and augments enzalutamide resistance in PCa (8).

Current evidence has suggested that lncRNA cancer susceptibility candidate 11 (CASC11) is upregulated in numerous types of cancer and promotes tumorigenesis (9). As well as having value in cancer diagnosis and prognostic prediction, CASC11 may also have potential as a target treatment in lung and liver cancer. Zhang *et al.* (10) reported that c-Myc enhanced promoter histone acetylation to increase CASC11 expression. Song *et al.* (11) demonstrated that CASC11 promoted the progression of hepatocellular carcinoma by means of EIF4A3-mediated E2F1 upregulation. CASC11 is highly expressed and acts as an oncogene in various human malignancies, and can also function as a competitive endogenous RNA (ceRNA) to exert influence on tumor-related genes by adhering to microRNA response elements or interacting with proteins (12). Furthermore, abnormal expression of CASC11 has been reported to be associated with overall survival of patients with tumors, and may be considered an important indicator of diagnosis and prognostic assessment (13). Previous studies have illustrated that CASC11 is associated with PCa proliferation through a ceRNA mechanism (14). However, the specific function of CASC11 has not been well investigated in the context of PCa development and the underlying mechanisms require elucidation.

The present study aimed to investigate the role of CASC11 in PCa and its potential oncogenic properties. The present findings supported the evidence regarding the biological functions of CASC11 and its underlying role in the Y-box binding protein 1 (YBX1)/p53 axis, which could be used as a promising therapeutic target for clinical treatment of PCa.

Materials and methods

Patients and tissue samples. A total of 66 paired PCa tissues and adjacent non-tumor tissues were obtained from patients who received surgery at The Second Affiliated Hospital of Anhui Medical University (Hefei, China) between May 2017 and May 2021. None of the patients received preoperative therapy. All samples were confirmed by experienced pathologists. The inclusion criteria were as follows: i) Patients met the World Health Organization diagnostic criteria for PCa (15); ii) patients had the capacity to provide informed consent. The exclusion criteria were as follows: i) Patient refusal; ii) patients with other diseases; iii) patients received treatment before admission. Tissues were snap-frozen in liquid nitrogen after resection and stored at -80°C . Written informed consent was provided by the participants. The present study was approved by the Ethics Committee of The Second Affiliated Hospital of Anhui Medical University (approval no. 2021-130). Patient information is shown in Table S1.

Cell culture and transfection. Human PCa cell lines (PC-3, DU145, 22Rv1 and LNCaP) and a human normal prostate epithelial cell line (RWPE-1) were obtained from The Cell Bank of Type Culture Collection of The Chinese Academy of Sciences. Cells were cultured in RPMI-1640 medium (Gibco;

Thermo Fisher Scientific, Inc.) containing 10% fetal bovine serum (FBS: Gibco; Thermo Fisher Scientific, Inc.) and 1% penicillin-streptomycin (Gibco; Thermo Fisher Scientific, Inc.) at 37°C with 5% CO_2 . For cell transduce, LNCaP and 22Rv1 cells at 60-70% confluence were plated in six-well plates at a density of 5×10^5 cells per well. The short hairpin RNA (shRNA) against CASC11 (sh-CASC11) and the shRNA-negative control (sh-NC) were designed and synthesized by Zorin, and were encoded within a CMV-PURO-MCS vector (Zorin). The shRNA sequences were as follows: sh-CASC11-1, 5'-GATCCG CCCACATCAAGCCTT-3'; sh-CASC11-2, 5'-GATCCGCCT TCATATAACAGCAGT-3'; sh-CASC11-3, 5'-GATCCGAAC TCACCAGCCAAGTT-3' and sh-NC, 5'-CGTCTACGTCCC GTGATACAATAA-3'. For gene overexpression, pcDNA3.1 vectors (Zorin) were subcloned with CASC11 (OE-CASC11) and an empty vector was used as a NC. LNCaP and 22Rv1 cells (5×10^5 cells per well) were transfected with 2 μg OE-CASC11 or the empty vector using Lipofectamine[®] 2000 (Invitrogen; Thermo Fisher Scientific, Inc.) at 37°C for 48 h according to the manufacturer's protocol. After 12 h, cells were subsequently used for experiments. The sh-NC and sh-CASC11 particles were packaged in 293T cells (cat. no. CRL-3216; American Type Culture Collection) using a 2nd generation system, with the ratio of lentiviral construct, packaging plasmid and envelope plasmid as 1 μg :900 ng:100 ng. The 293T cells were then cultured in DMEM (Gibco; Thermo Fisher Scientific, Inc.) supplemented with 10% FBS in 5% CO_2 at 37°C for 48 h. The cultured media were centrifuged at $1,000 \times g$ for 5 min at room temperature to remove packaging cells and the supernatant containing viral particles was collected. Lentiviral infection (multiplicity of infection, 10) was performed to knock down CASC11 in LNCaP and 22Rv1 cells. For the establishment of stable cell lines, cells were infected with lentivirus along with polybrene (5 $\mu\text{g}/\text{ml}$) and screened with 2 $\mu\text{g}/\text{ml}$ puromycin (MilliporeSigma) for 2 weeks. Subsequently, surviving cells were maintained in complete medium with puromycin (0.5 $\mu\text{g}/\text{ml}$) and the stable cell lines were used for subsequent experiments. Transfection efficiency was validated by reverse transcription-quantitative PCR (RT-qPCR).

LNCaP and 22Rv1 cells (1×10^6) were also transfected with corresponding YBX1 small interfering RNA (siRNA/si, 20 μM), si-NC (20 μM), empty vector (50 nM) and YBX1 overexpression plasmid (OE-YBX1, 50 nM) (Sangon Biotech Co., Ltd.) within pcDNA3.1 vector (Sangon Biotech Co., Ltd.) using Lipofectamine 2000 transfection reagent at 37°C for 48 h. A total of 48 h following transfection, cells were subjected to subsequent experiments. The target sequences were as follows: YBX1-siRNA, 5'-CAGUUCAAGGCAGUAAUAUGCA-3'; si-NC, 5'-CGUGAACUAAAGUCGAGUACUAA-3'. Western blotting was used to validate the efficiency of transfection.

RT-qPCR. Total RNA was extracted from cells and tissues using TRIzol[®] reagent (Invitrogen; Thermo Fisher Scientific, Inc.). The A260/A280 ratio was used to assess RNA purity. A total of 2 μg RNA was reverse transcribed into cDNA using the PrimeScript RT Reagent kit (Takara Biotechnology Co., Ltd.) according to the manufacturer's protocol. Expression levels were determined by qPCR using SYBR Premix Ex Taq (Takara Biotechnology Co., Ltd.). The thermocycling conditions were as follows: Initial denaturation at 95°C for 30 sec;

40 cycles of 10 sec at 95°C, 30 sec at 60°C and 72°C for 15 sec; with a final extension cycle at 72°C for 5 min. GAPDH was used as an internal control. Fold-changes were calculated using the $2^{-\Delta\Delta C_q}$ method (16). The primer sequences were as follows: CASC11, forward 5'-ACCCTATGGAGAACCGAGAC-3' and reverse 5'-GAGGACCAACTCAGTAGGAAAT-3'; GAPDH, forward 5'-AATGGGCAGCCGTTAGGAAA-3' and reverse 5'-GCCCAATACGACCAAATCAGAG-3'.

Cell viability assay. Cell viability was detected using the Cell Counting Kit 8 (CCK-8; Sangon Biotech Co. Ltd.). Briefly, LNCaP and 22Rv1 cells were cultured in 96-well plates (2,000 cells/well). Cell viability was measured every 24 h, whereby 10 μ l CCK-8 solution was added to each well and incubated for 2 h at 37°C. For assessing the biosafety of PBAE, different concentrations of PBAE (0, 5, 10, 15, 20, 25 and 30 μ g/ml) were added to LNCaP and 22Rv1 cells for 24 h at 37°C. The absorbance was measured spectrophotometrically at an optical density of 450 nm using a SpectraMax i3X (Molecular Devices, LLC). The experiments were repeated three times.

Cell colony formation assay. A total of 500 cells were grown in each well of a 6-well plate for ~2 weeks at 37°C and 5% CO₂ until colony formation was evident. Cells were fixed with methanol for 10 min at room temperature and stained with 0.5% crystal violet for 10 min at room temperature, and images were captured for cell counting. The colonies were counted using ImageJ software (version 1.5; National Institutes of Health). The experiments were repeated three times.

Cell migration assay. The cell migration assay was conducted using a 24-well plate with chamber inserts (pore size, 8 μ m; Corning, Inc.). Cells (1×10^5) in 200 μ l serum-free medium were added to the upper chamber, whereas the lower chamber contained 800 μ l medium supplemented with 10% FBS. After 24 h of incubation at 37°C and 5% CO₂, cells on the lower surface of the membrane were fixed with 4% paraformaldehyde for 20 min at room temperature and stained with Giemsa for 15 min at room temperature. The images were acquired with an inverted light microscope (Olympus Corporation) and counted using ImageJ software. The experiments were repeated three times.

Wound healing assay. The wound healing assay was conducted using a 6-well plate. When the cell monolayers reached 80% confluence, they were scratched using a 200- μ l pipette tip. Subsequently, cells were cultivated in fresh serum-free medium at 37°C and 5% CO₂. Images of cell migration were captured at the same locations at 0 and 24 h using an inverted light microscope (Olympus Corporation), and the wound area was estimated using ImageJ software. Wound healing rate was determined as follows: Wound healing rate (%) = [(wound distance at 0 h - wound distance at 24 h) / (wound distance at 0 h)] x 100. The experiments were repeated three times.

5-ethynyl-2'-deoxyuridine (EdU) proliferation assay. To measure cell proliferation, cells were cultured in 24-well plates and treated with EdU for 4 h according to the protocol of the EdU Kit (Guangzhou RiboBio Co., Ltd.). Cells were then fixed

with 4% paraformaldehyde for 30 min at room temperature and permeabilized with 0.5% Triton X-100 for 10 min at room temperature (MilliporeSigma). Images were captured using a fluorescence microscope. The experiments were repeated three times.

RNA immunoprecipitation (RIP). RIP experiments were performed using a Magna RIP RNA Binding Protein Immunoprecipitation Kit (cat. no. 17-700; MilliporeSigma) according to the manufacturer's instructions. Briefly, 1×10^7 cells were collected, centrifuged at 4°C for 5 min at 1,000 x g, washed with pre-cooled phosphate-buffered saline (PBS) and lysed in 800 μ l RIP buffer (MilliporeSigma). Subsequently, 50 μ l protein A/G magnetic beads (cat. no. 26162; Pierce; Thermo Fisher Scientific, Inc.) were resuspended in 1 ml RIP wash buffer before being incubated for 1 h at room temperature with YBX1 (cat. no. ab76149; 1:50; Abcam) or IgG (cat. no. ab200699; 1:1,000; Abcam) antibodies. The beads-antibody complex was then mixed with RIP buffer and 100 μ l cell lysate at 4°C overnight. The beads were then washed with RIP wash buffer three times. Subsequently, proteinase K was added to each immunoprecipitated product and incubated for 30 min at 55°C to digest the protein. Following centrifugation at 4°C for 5 min at 1,000 x g, total RNA was extracted for agarose gel electrophoresis on 2% agarose gels and RT-qPCR analysis. Bands were visualized by staining with ethidium bromide (MilliporeSigma). The experiments were repeated three times.

RNA pull-down and mass spectrometry (MS). CASC11 sense (5'-GGGAAGGGACAACACTAAGCAAAA-3') and antisense (5'-AACGGACGGAAACATAAAAAGGCG-3') were amplified *in vitro* using the MAXIscript™ T7 Transcription Kit (Thermo Fisher Scientific, Inc.) and labeled via desulfurization biotinylation using a Pierce™ RNA 3' End Desthiobiotinylation kit (Thermo Fisher Scientific, Inc.) before being incubated with 40 μ l streptavidin magnetic beads (cat. no. 88816; Thermo Fisher Scientific, Inc.) for 2 h at room temperature. Cell extracts were prepared from 1×10^7 cells in 900 μ l Pierce IP Lysis Buffer (Thermo Scientific, Inc.), then mixed with biotin-labeled CASC11 at 4°C for 1 h. Biotin Elution Buffer (Thermo Fisher Scientific, Inc.) was added to collect the RNA complex pulled down. All experiments were carried out as recommended by the manufacturer of the Pierce Magnetic RNA-Protein Pull-Down kit (Thermo Fisher Scientific, Inc.), and the proteins that engaged with the sense or antisense CASC11 were identified. After elution, lncRNA-associated proteins were separated by SDS-PAGE on 10% gels and stained with silver for 2 min at room temperature. Subsequently, the retrieved proteins were analyzed using MS. MS analysis was performed on a Q Exactive mass spectrometer (Thermo Scientific, Inc.) that was coupled to Easy nLC (Proxeon Biosystems, now Thermo Fisher Scientific) for 60 min. The mass spectrometer was operated in positive ion mode.

Fluorescence in situ hybridization (FISH). LNCaP and 22Rv1 cells were cultured in confocal dishes (Corning, Inc.). Oligonucleotide modified Cy3-labeled probes for human lncRNA CASC11 (5'-TTATGCGGTTGAATAGTCACCTCT

G-3') were designed and obtained from Shanghai GenePharma Co., Ltd. A cy3-labeled 18S rRNA was used as a positive control (Shanghai GenePharma Co., Ltd.). Experimental procedures were carried out according to the instructions included in the RibTM FISH kit (Guangzhou Ribobio Co., Ltd.). Briefly, the cell suspension (1×10^4) was pipetted onto autoclaved glass slides. The slides were washed in PBS and fixed in 4% paraformaldehyde for 10 min at room temperature and permeabilized with 0.3% Triton X-100 for 5 min at 4°C. Hybridization was performed at 37°C overnight in a dark moist chamber. After being washed three times in saline sodium citrate buffer, the coverslips were sealed with parafilm containing DAPI. The images were acquired using a confocal microscope (LSM900; Carl Zeiss AG). The experiments were repeated three times.

Western blot analysis. Western blotting was carried out based on a standard protocol. Briefly, cells were washed with chilled PBS and lysed with RIPA lysis buffer (Beyotime Institute of Biotechnology). The concentration of each protein was determined using a BCA protein assay kit (Pierce; Thermo Fisher Scientific, Inc.). Total protein extracts (20 μ g) were separated by SDS-PAGE on 10% gels and transferred onto PVDF membranes. The membranes were blocked with 5% nonfat dry milk at room temperature for 2 h and blotted with primary antibodies against Cyclin A2 (cat. no. 67955; 1:1,000; Cell Signaling Technology, Inc.), CDK2 (cat. no. 18048; 1:1,000; Cell Signaling Technology, Inc.), CDK4 (cat. no. 12790; 1:1,000; Cell Signaling Technology, Inc.), p53 (cat. no. 2527; 1:1,000; Cell Signaling Technology, Inc.), p21 (cat. no. 2947; 1:1,000; Cell Signaling Technology, Inc.), YBX1 (cat. no. ab76149; 1:1,000; Abcam) and GAPDH (cat. no. ab8245; 1:2,000; Abcam) at 4°C overnight. The membranes were then washed three times with PBS and incubated with goat anti-rabbit IgG secondary antibody (cat. no. ab7090; 1:10,000; Abcam) and goat anti-mouse IgG secondary antibody (cat. no. ab6789; 1:10,000; Abcam) for 1 h at room temperature. Signals from membranes were measured using ECL Substrate (Bio-Rad Laboratories, Inc.). GAPDH was used as an internal reference. Semi-quantitative analysis was performed using ImageJ software. The experiments were repeated three times.

Flow cytometry. For cell cycle distribution analysis, 1×10^5 cells were collected and fixed in 70% pre-cooled ethanol overnight at 4°C. Subsequently, cells were treated with RNase A (Beyotime Institute of Biotechnology) at 37°C for 30 min and stained with 500 μ l propidium iodide (Beyotime Institute of Biotechnology) at room temperature for 30 min in the dark. The percentage of cells in each cycle phase was calculated by flow cytometry (BD FACSCanto II; BD Biosciences). Data were analyzed by FlowJo version 10 (FlowJo LLC). The experiments were repeated three times.

RNA-sequencing (RNA-seq) processing. Total RNA was extracted from sh-NC and sh-CASC11 cells using TRIzol. A NanoDrop (NanoDrop; Thermo Fisher Scientific, Inc.) was used to measure the quantity and quality of RNA. The DNA library was constructed using an Illumina Nextera XT DNA Library Prep Kits (Illumina, Inc.), based on the KAPA stranded RNA-Seq Library, and enrichment of RNA was performed with oligo(dT) magnetic beads. Agilent 4200

(Agilent Technologies, Inc.) was used to detect the quality of the constructed library. To select cDNA fragments of the preferred 200 bp in length, the library fragments were purified using the AMPure XP system (Beckman Coulter, Inc.). Libraries were validated by electrophoresis, pooled, and sequenced on an Illumina NovaSeq 6000 (150 base pairs, paired ends; Illumina, Inc.). The RNA sequencing was performed by HaploX Biotechnology. Differentially expressed mRNAs were identified according to $|\log_2(\text{Fold Change})| > 1$ and $P < 0.05$ by R package EdgeR (version 3.6.3; <http://bioconductor.org/packages/edgeR/>).

Preparation of poly (β -amino ester) (PBAE)/si-CASC11 nanocomplexes. PBAE was purchased from Xi'an Ruixi Biotechnology Co., Ltd. CASC11 siRNA (siCASC11; sequence: 5'-GCCCAUCAUAAGCCUUCAU-3') was synthesized by Shanghai GenePharma Co., Ltd. Seven complexes with different ratios (1, 5, 10, 20, 40, 60 and 80 of PBAE to si-CASC11 by weight) were prepared. Subsequently, PBAE solutions of different concentrations were vortexed along with a si-CASC11 solution to obtain PBAE/si-CASC11 nanocomplexes (17,18). PBAE/si-CASC11 nanocomplexes were mixed with loading buffer and underwent electrophoresis on 2% agarose gels; si-CASC11 alone was used as a control. Electrophoresis was performed at 130 V for 15 min and the gel was imaged on the Tanon Gel image system (Tanon Science & Technology Co., Ltd). The particle size of the nanocomplexes was determined using a particle size potentiometer (Nano ZS90; Malvern Panalytical; Spectris Plc).

Transmission electron microscopy (TEM). PBAE/siRNA nanoparticles were formed and then droplets of the sample (5 μ l) were applied to hydrophilized carbon-covered copper grids (300 mesh) for 30 min. The sample was subsequently rinsed with contrasting material (1% uranyl acetate, pH 4.5). The remaining stain solution was removed with a filter paper and air-dried. TEM microstructure was determined using a high contrast TEM (JEM2010; JEOL, Ltd.) at 120 kV.

In vivo experiments. A total of 36 (n=6 mice/group; weight, 20-25 g; age, 4-6 weeks) male BALB/C nude mice were purchased from Weitong Lihua Laboratory Animal Technology Co., Ltd. and were maintained in a specific pathogen-free-grade research center (temperature, 28°C; humidity, 50%; light/dark cycle, 10/14-h cycle), with free access to food and water. The mice were divided into the following groups: sh-NC group; sh-CASC11-1 group; sh-CASC11-2 group; saline group; si-CASC11 group; PBAE/si-CASC11 group. The animal experiment was approved by the Animal Research Ethics Committee of The Second Affiliated Hospital of Anhui Medical University (approval no. 2021080). A total of 5×10^6 sh-NC and sh-CASC11 22Rv1 cell lines were injected subcutaneously into the nude mice. The weight and tumor size were measured every 4 days. Tumor volume was calculated as follows: $\text{Volume (mm}^3\text{)} = 0.5 \times \text{width}^2 \times \text{length}$. After 4 weeks, the mice were euthanized by cervical dislocation. For comparing the antitumor effect of si-CASC11 and PBAE/si-CASC11, 5×10^6 22Rv1 cell lines were injected subcutaneously into the nude mice and the xenograft tumors developed 4 weeks after injection. Saline, si-CASC11 or

PBAE/si-CASC11 nanocomplexes were injected intratumorally (50 μ l) into the three groups, twice a week for 3 weeks. The mice were euthanized by cervical dislocation and sacrifice was confirmed when the mice had stopped breathing and did not respond to stimulation. Finally, tumor tissues were carefully resected, images were captured and they were assessed using hematoxylin and eosin (H&E) staining and immunohistochemistry (IHC).

H&E staining. Mouse tissues were fixed in 10% formalin solution for 12 h at room temperature and paraffin-embedded, then cut and mounted on slides (4 μ m). In a descending alcohol series, the tissue sections were dewaxed and rehydrated. The slides were then stained with hematoxylin for 2 min at room temperature. Subsequently, the slides were washed in water for 10 min and then stained with eosin for 1 min at room temperature after differentiation in acid alcohol. Images were obtained using a light microscope (Olympus Corporation).

IHC. Tumor tissues were embedded in paraffin and sectioned (4 μ m) after being fixed with 4% paraformaldehyde at 4°C for 24 h. Dewaxed sections were rehydrated with ethanol at room temperature for 15 min and then incubated with 3% H₂O₂ for 10 min to inhibit endogenous peroxidases. For antigen retrieval, citrate buffer (pH 6.0) was applied for 20 min at 95°C. Slides were incubated with primary antibodies overnight at 4°C, against Ki-67 (cat. no. ab15580; 1:200; Abcam). Subsequently, the sections were incubated with HRP-conjugated secondary antibody (cat. no. ab6721; 1:1,000; Abcam) for 40 min at 37°C. The sections were rinsed three times using TBS with 0.1% Tween-20 for 5 min. DAB (MilliporeSigma) was also applied at room temperature for 15 min and the tissues were observed under a light microscope (BX53; Olympus Corporation). The experiments were repeated three times.

Bioinformatics analysis. The expression levels of CASC11 in PCa were obtained from The Cancer Genome Atlas (TCGA) database (<https://cancergenome.nih.gov/>) and Gene Expression Omnibus (GEO) database (<https://www.ncbi.nlm.nih.gov/geo/>). The GSE46602 and GSE55945 datasets were assessed using the GEO database (19,20). The expression of CASC family members in prostate tumors and normal tissue samples, as well as their association with Gleason scores, were analyzed by Gene Expression Profiling Interactive Analysis (<http://gepia.cancer-pku.cn/>). Kyoto Encyclopedia of Genes and Genomes (KEGG) analysis (<https://www.genome.jp/kegg/>) was used to identify the biological functions of CASC11. $P < 0.05$ and $\log_2(\text{fold change}) > 1$ were set as the cut-off criteria. The heatmap plot was generated using R heatmap package (<http://CRAN.R-project.org/package=heatmap>).

Statistical analysis. GraphPad Prism 8 (GraphPad Software, Inc.) was used for statistical analysis. Unpaired Student's t-test was used for the comparisons between two groups. Paired Student's t-test was used to analyze differences between paired tumor and paracancerous tissues. For comparisons between three or more groups, one-way ANOVA was performed followed by Dunnett's or Tukey's multiple comparison test. Data are presented as the mean \pm SD, or as scatter dot plots, box plots or violin plots, where the lines represent the median.

Two-tailed $P < 0.05$ was considered to indicate a statistically significant difference.

Results

LncRNA CASC11 expression is upregulated in PCa. Bioinformatics analysis was performed to determine the expression of CASC11 in PCa in TCGA dataset. Among the CASC family, the expression levels of CASC11 in TCGA dataset were increased in prostate tumor tissues compared with those in normal prostate tissues (Fig. 1A). In addition, CASC11 expression was elevated in tumor samples from patients with PCa and high Gleason scores (Fig. 1B). Moreover, the R package was used to analyze two GEO datasets (GSE46602 and GSE55945) to identify the expression of CASC11; the results revealed that CASC11 had a tendency to increase in tumor specimens compared with in normal tissues. (Fig. 1C and D). To further verify the oncogenic potential of CASC11, the mRNA expression levels of CASC11 were analyzed in prostate tumor samples obtained from The Second Affiliated Hospital of Anhui Medical University, and the results revealed that the expression levels were significantly upregulated in tumor samples compared with those in normal prostate specimens (Fig. 1E). Consistent with these data, analysis of PCa cell lines (22Rv1, DU145, PC-3 and LNCaP) and RWPE-1 non-tumorigenic prostate epithelial cells revealed that CASC11 was upregulated in cancer cells compared with in RWPE-1 cells (Fig. 1F). These data indicated that CASC11 may have a carcinogenic role in PCa. Since CASC11 is expressed highest in LNCaP and 22Rv1 cells, these two cell lines were used for subsequent analyses. Furthermore, FISH assay revealed that CASC11 was mainly distributed in the nucleus of LNCaP and 22Rv1 cells (Fig. 1G).

CASC11 promotes the proliferation and migration of PCa cells in vitro. Loss-of-function and gain-of-function assays were conducted in PCa cells to explore the biological function of CASC11. CASC11 was knocked down in LNCaP and 22Rv1 cells using a highly efficient shRNA-lentivirus and an overexpression plasmid system was used to upregulate the expression of CASC11 in these cell lines (Fig. 2A and B). Notably, of the three shRNAs, sh-CASC11-1 and sh-CASC11-2 displayed the highest efficiency; therefore, these were used for further experiments. CCK-8, colony formation and EdU assays revealed that knockdown of CASC11 significantly inhibited the proliferative capacity of PCa cells. By contrast, overexpression of CASC11 significantly enhanced the proliferation of PCa cells (Fig. 2C-N). Furthermore, wound healing and Transwell assays were performed to assess cell motility; the results revealed that CASC11 knockdown inhibited the migratory ability of PCa cells, whereas CASC11 overexpression promoted cell migration (Fig. 3A-J). Taken together, these data indicated that CASC11 could promote the proliferation and migration of PCa cells.

CASC11 promotes PCa cell progression by affecting G₁/S transition of the cell cycle. In order to further explore the underlying mechanism of action of CASC11, flow cytometry was used to analyze the cell cycle progression of PCa cells. Compared with in the control group, the proportion

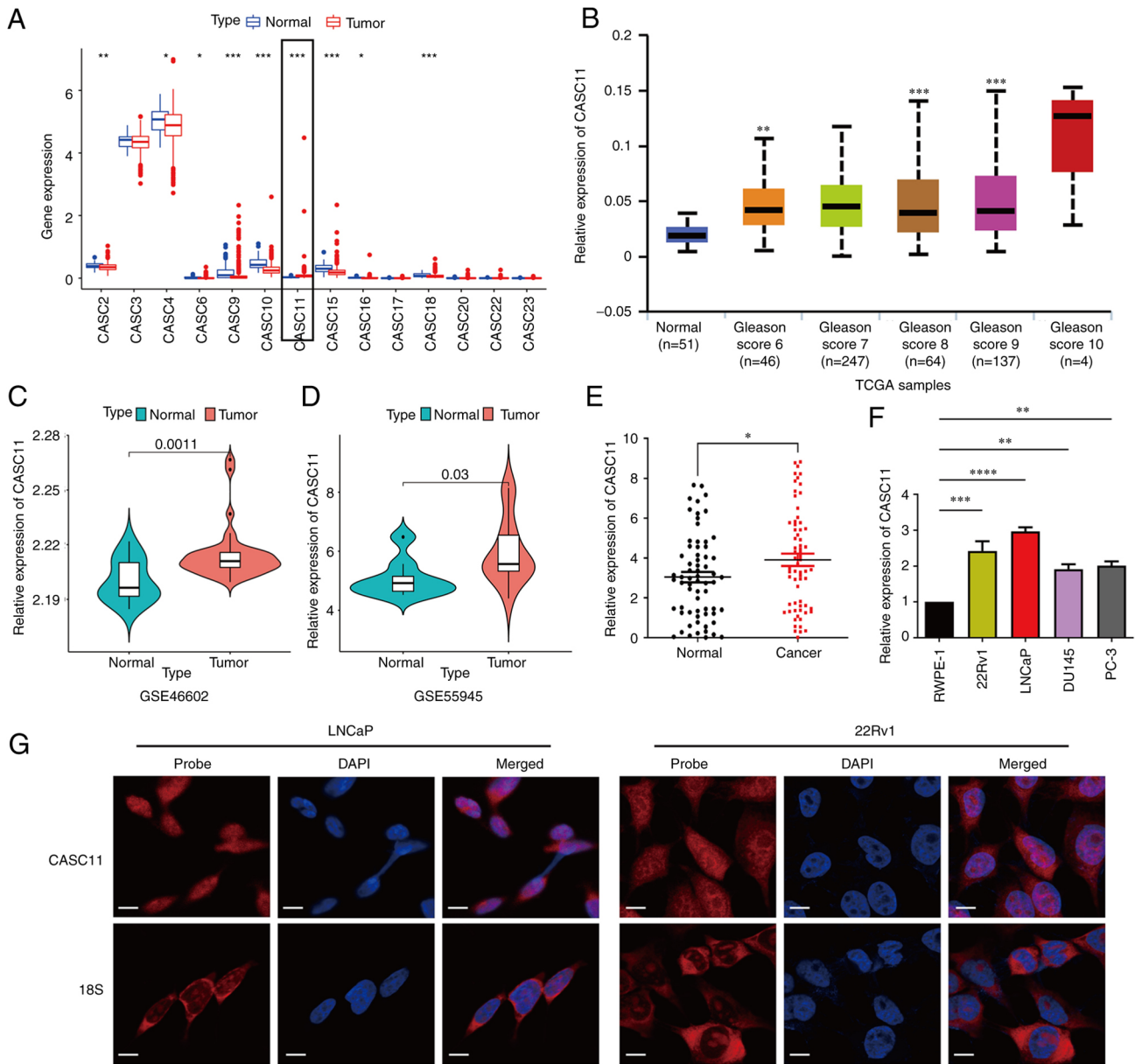


Figure 1. Long non-coding RNA CASC11 expression is upregulated in PCA. (A) Differential expression profile of non-coding CASC gene family members in PCA samples and normal tissues. (B) Expression of CASC11 in prostate tumor and normal tissue samples with different Gleason scores in TCGA dataset. (C and D) Expression of CASC11 in prostate tumor and normal tissues in GSE46602 and GSE55945 datasets. (E) Expression of CASC11 in 66 paired prostate tumor and normal tissue samples. (F) Expression levels of CASC11 in PCA cell lines (LNCaP, PC-3, DU145 and 22Rv1) and a prostate epithelial cell line (RWPE-1). (G) Fluorescence *in situ* hybridization analysis of CASC11 in LNCaP and 22Rv1 cells. DAPI was used to stain the nuclei, and 18S was used as a positive control for cytoplasmic staining. Scale bar, 50 μ m. * P <0.05, ** P <0.01, *** P <0.001, **** P <0.0001 vs. normal or as indicated. CASC11, cancer susceptibility candidate 11; PCA, prostate cancer; TCGA, The Cancer Genome Atlas.

of cells in G_1 phase was significantly increased, whereas the proportion of cells in S phase was decreased after CASC11 knockdown (Fig. 4A-C). By contrast, the overexpression of CASC11 led to an increase in the number of cells in S phase (Fig. 4D-F). The results of flow cytometry indicated that CASC11 could affect cell cycle progression in PCA; CASC11 knockdown caused cell cycle arrest at G_1 phase, whereas CASC11 overexpression induced cell cycle arrest at S phase. Subsequently, the expression levels of three proteins associated with the G_1 /S phase were assessed. The results revealed that the expression levels of CyclinA2, CDK2 and CDK4 were downregulated after CASC11 knockdown and upregulated in CASC11-overexpressed PCA cells (Fig. 4G and H). These

data indicated that CASC11 promoted PCA cell progression by mediating the G_1 /S transition in the cell cycle.

CASC11 knockdown inhibits PCA cell tumorigenesis in vivo. To verify the effects of CASC11 knockdown on PCA tumorigenesis *in vivo*, 22Rv1 cells transduced with sh-CASC11-1, sh-CASC11-2 or sh-NC were injected subcutaneously into nude mice. As presented in Fig. 5A, tumors implanted in the sh-CASC11 group were smaller than those in the sh-NC group. Additionally, the tumor volume and tumor weight were significantly lower in the sh-CASC11 group (Fig. 5B and C). Immunohistochemical staining of Ki-67 indicated that tumor proliferation was markedly reduced in the sh-CASC11 group (Fig. 5D and E).

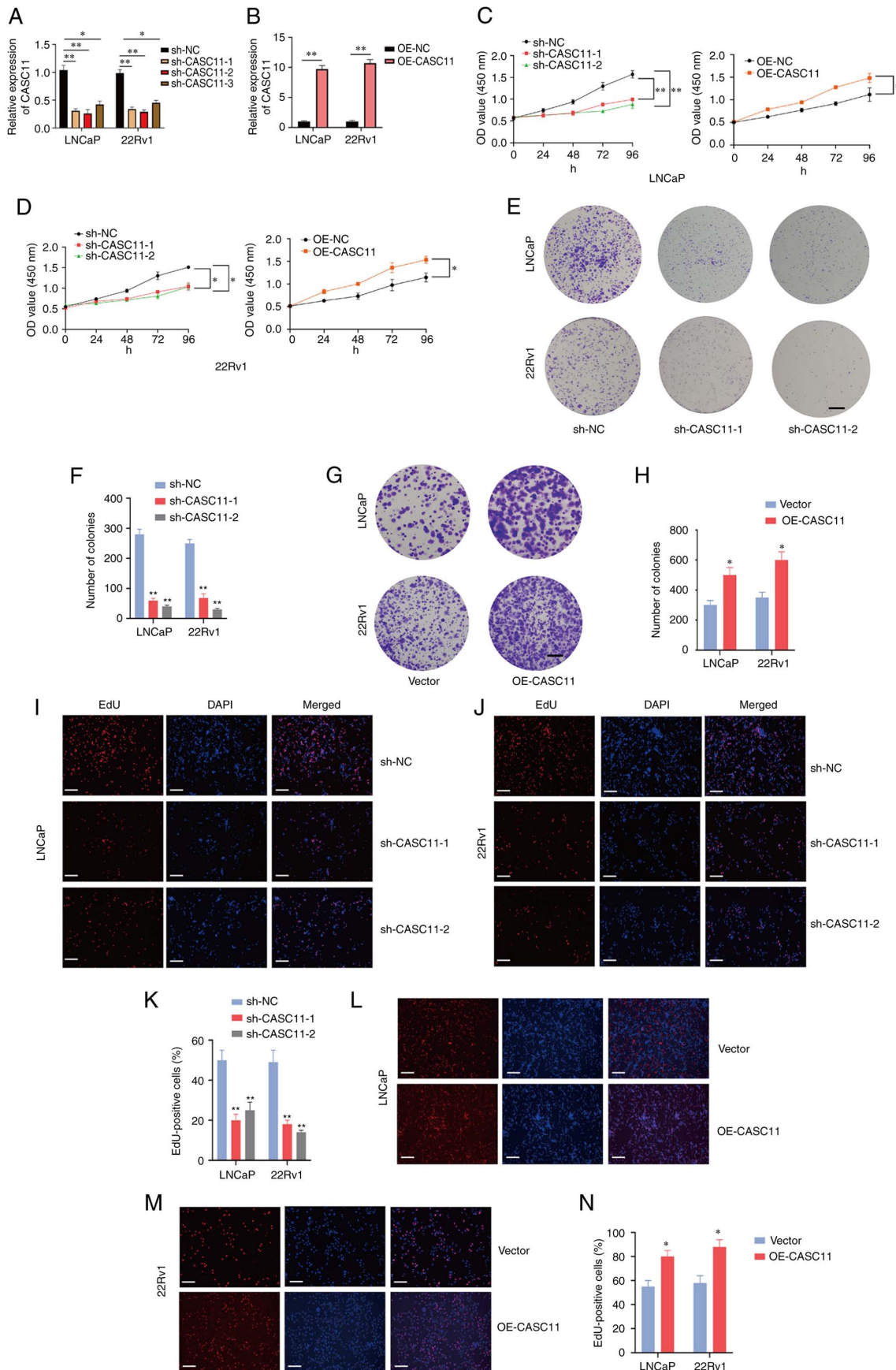


Figure 2. CASC11 promotes proliferation of PCa cells. Expression levels of CASC11 were (A) significantly downregulated in sh-CASC11-infected PCa cells and (B) significantly upregulated in OE-CASC11-transfected cells. (C and D) Cell Counting Kit-8 assay was used to investigate the proliferative effects of CASC11 knockdown or overexpression on PCa cells. (E-H) Colony formation assay was applied to investigate the proliferative ability of PCa cells. Scale bar, 500 μ m. (I-N) EdU assay was applied to investigate the proliferative effects of CASC11 knockdown or overexpression in PCa cells. Scale bar, 100 μ m. * P <0.05, ** P <0.01 vs. sh-NC or vector, or as indicated. CASC11, cancer susceptibility candidate 11; EdU, 5-ethynyl-2'-deoxyuridine; NC, negative control; OE-CASC11, CASC11 overexpression plasmid; PCa, prostate cancer; sh, short hairpin.

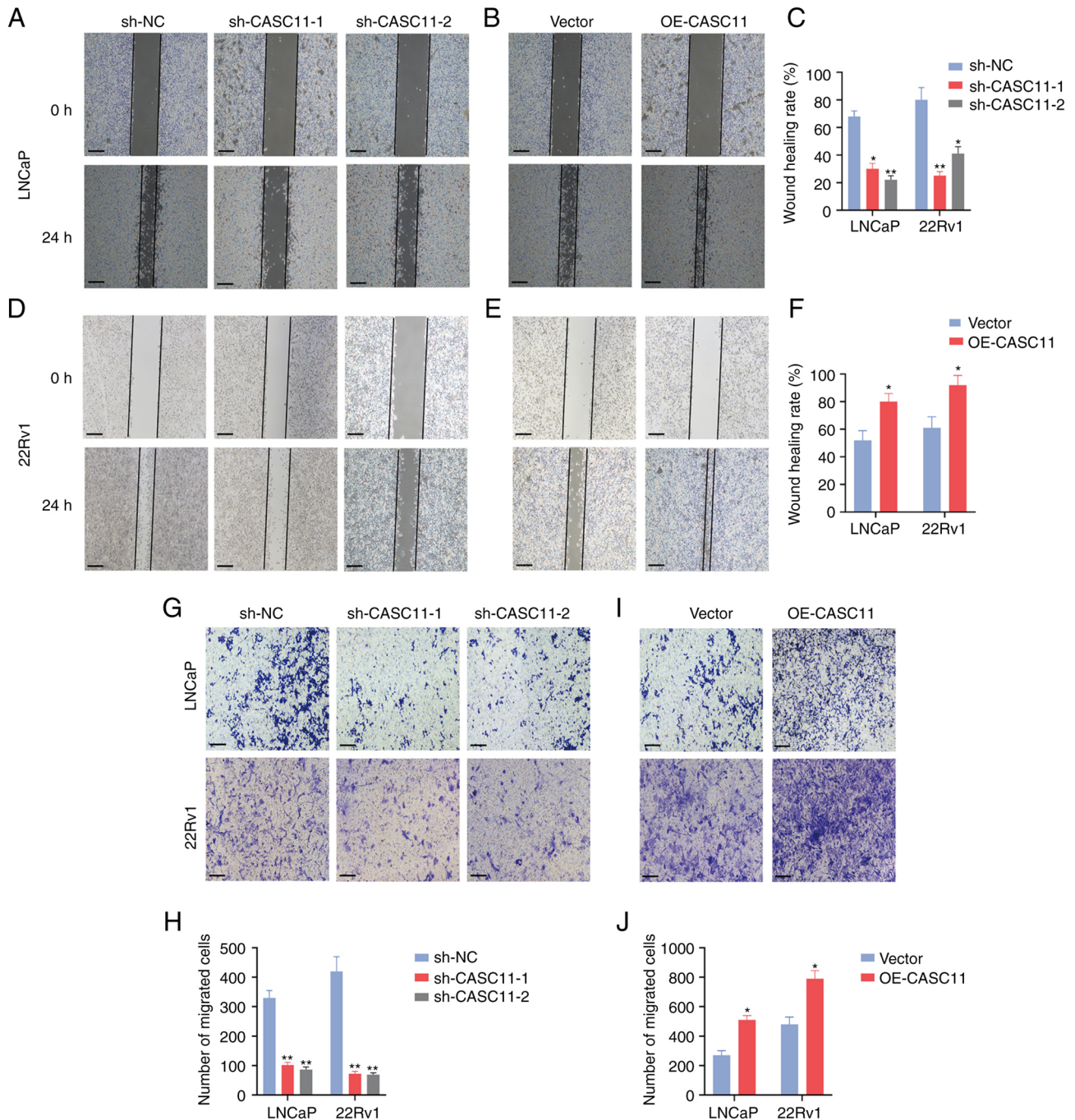


Figure 3. CASC11 promotes migration of PCa cells. (A-C) CASC11 knockdown attenuated cell migration in LNCaP cells, whereas CASC11 overexpression exerted the opposite effect. (D-F) CASC11 knockdown attenuated cell migration in 22Rv1 cells, whereas CASC11 overexpression exerted the opposite effect. (G and H) Transwell assay demonstrated that CASC11 knockdown inhibited cell migration in LNCaP and 22Rv1 cells. (I and J) Transwell assay demonstrated that CASC11 overexpression promoted cell migration in LNCaP and 22Rv1 cells. Scale bar, 100 μ m. * $P < 0.05$, ** $P < 0.01$ vs. sh-NC or vector. CASC11, cancer susceptibility candidate 11; NC, negative control; OE-CASC11, CASC11 overexpression plasmid; PCa, prostate cancer; sh, short hairpin.

CASC11 promotes PCa progression by attenuating p53 signaling. To further understand the underlying mechanism of the effects of CASC11 on PCa tumorigenesis, RNA-seq analysis of 22Rv1 cells following CASC11 gene silencing was performed and a heat map displayed the differentially expressed genes between sh-NC and sh-CASC11 groups (Fig. 6A). As shown in Fig. S1A, KEGG pathway analysis demonstrated that CASC11 was associated with the 'cell cycle' and 'p53 signaling' pathways (ranking 1 and 2, $P < 0.05$), which are closely related to cell proliferation and apoptosis. To

validate the role of p53 signaling, the expression levels of p53 and p21, which is a downstream gene of p53 signaling, were examined by western blotting. CASC11 silencing induced an increase in p53 and p21 expression, as expected (Fig. 6B). According to these results, it was suggested that impaired p53 signaling may contribute to the biological function of CASC11 in regulating PCa progression.

CASC11 suppresses p53 signaling in PCa cells through interaction with YBX1. Analysis of protein interactions with

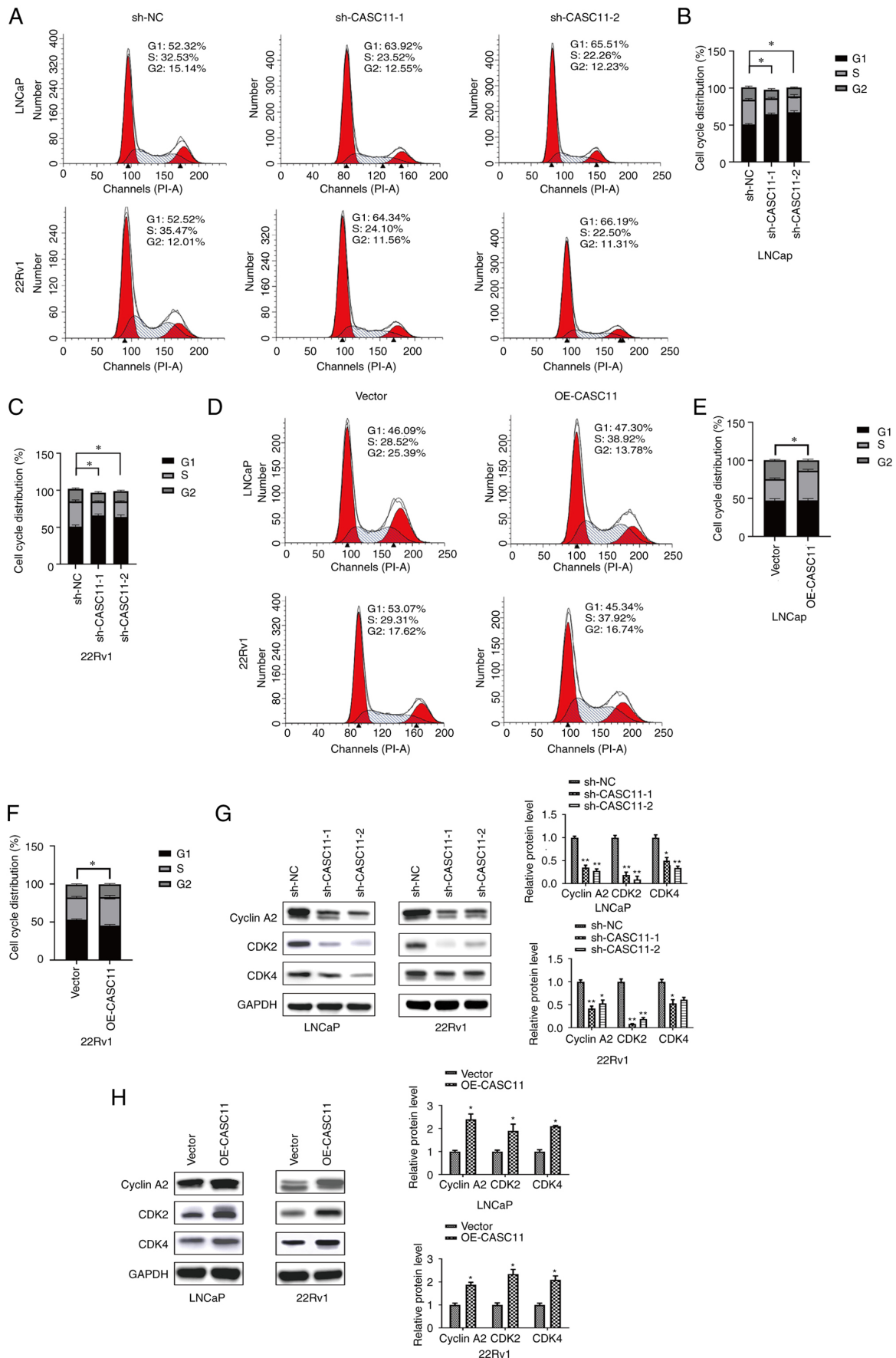


Figure 4. CASC11 promotes prostate cancer cell proliferation by stimulating G₁/S cell cycle transition. (A-C) CASC11 knockdown resulted in cell cycle arrest at G₁ phase in LNCaP and 22Rv1 cells. *P<0.05 vs. sh-NC (G₁ and S stages). (D-F) CASC11 overexpression resulted in cell cycle arrest at S phase in LNCaP and 22Rv1 cells. *P<0.05 vs. sh-NC (S stage). Western blot analysis was used to detect the effects of CASC11 (G) knockdown and (H) overexpression on the expression levels of cell cycle-associated proteins in LNCaP and 22Rv1 cells. *P<0.05, **P<0.01 vs. sh-NC or vector, or as indicated. CASC11, cancer susceptibility candidate 11; NC, negative control; OE-CASC11, CASC11 overexpression plasmid; sh, short hairpin.

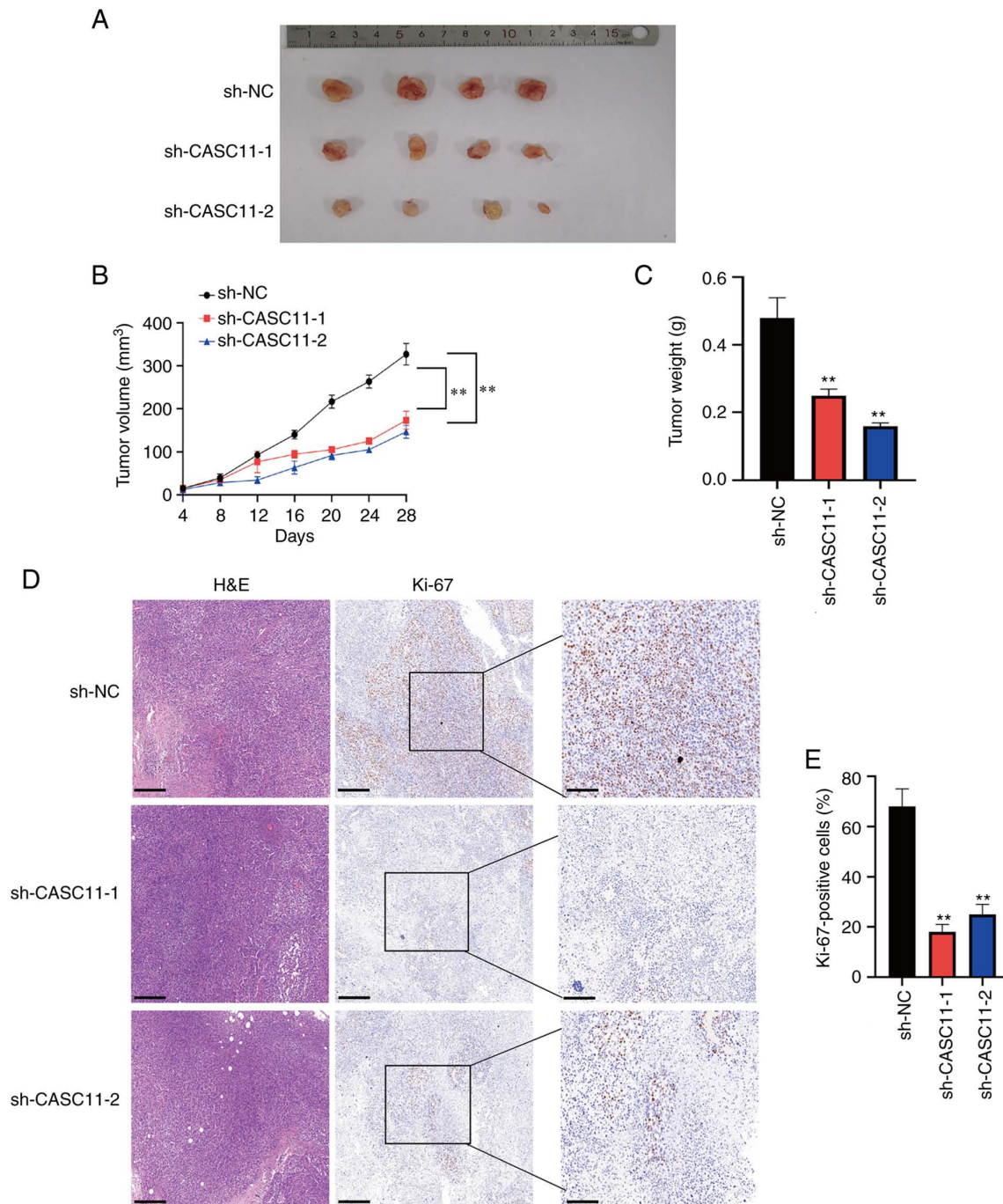


Figure 5. CASC11 knockdown inhibits prostate cancer cell tumorigenesis *in vivo*. (A) Following stable transduction of sh-NC, sh-CASC11-1 and sh-CASC11-2 into 22Rv1 cells, the cells were then injected into nude mice. (B) Tumor volumes were measured every 4 days following injection. (C) Tumor weight is presented as the mean \pm SD. (D and E) Subcutaneous tumor proliferation was inhibited in the sh-CASC11 group, as determined by immunohistochemical analysis of Ki-67. Scale bars, 100 and 200 μ m. ** $P < 0.01$ vs. sh-NC or as indicated. CASC11, cancer susceptibility candidate 11; H&E, hematoxylin and eosin; NC, negative control; sh, short hairpin.

CASC11 using RNA-protein pull-down was used to better elucidate the pathway governing the CASC11 regulatory network. By silver staining of SDS-PAGE gels, it was revealed that CASC11 was specifically bound to protein bands ranging in size from 30 to 150 kDa (Fig. 6C), and the primary protein involved in CASC11 interaction was identified as YBX1 by MS (Fig. S1B). Furthermore, the interaction between YBX1 and CASC11 was further assessed by RIP. RIP assay confirmed that CASC11 could bind YBX1 (Fig. 6D and E). Moreover, a downregulation in the protein expression levels of

YBX1 was detected upon CASC11 knockdown in PCa cells, whereas the opposite results were detected in cells where CASC11 was overexpressed (Fig. 6F and G). In general, these results indicated that CASC11 inhibited p53 signaling through binding with YBX1.

YBX1 knockdown reverses the carcinogenic effects of CASC11 promotion on PCa cells. For further investigating whether CASC11 exerted its biological function by binding to YBX1, a rescue assay between CASC11 and YBX1 was performed.

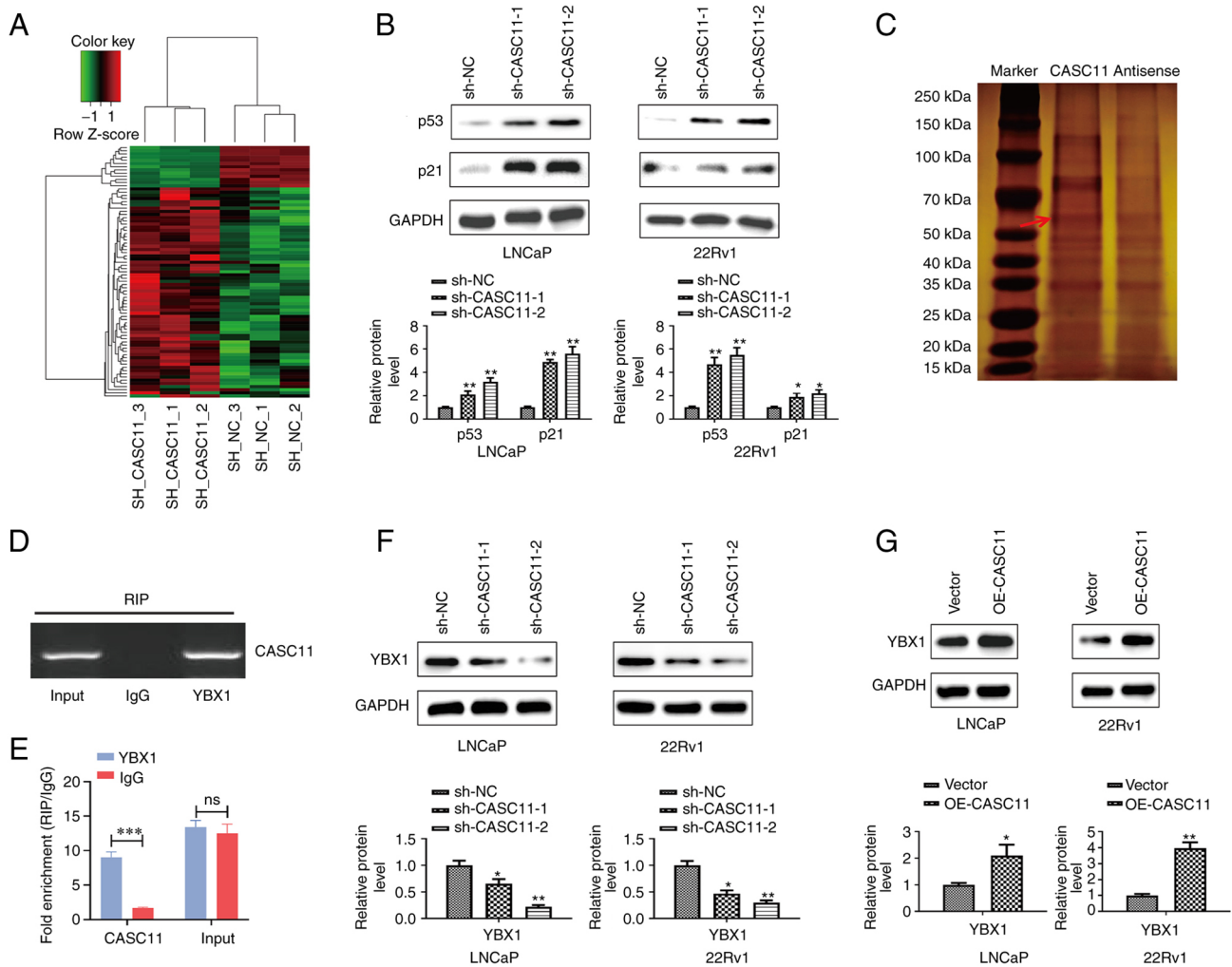


Figure 6. CASC11 suppresses p53 signaling in prostate cancer cells by binding with YBX1. (A) Heat map displaying differentially expressed genes in sh-CASC11 groups and sh-NC groups by RNA sequencing. (B) Protein expression levels of p53 and p21 were measured by western blotting when CASC11 was knocked down in LNCaP and 22Rv1 cells. (C) SDS-PAGE gel stained with silver to show separated proteins. (D and E) Using the YBX1 or IgG antibody, reverse transcription-quantitative PCR was used to examine RNA enrichment in RIP assay. (F and G) Protein expression levels of YBX1 were measured by western blotting when CASC11 was knocked down or overexpressed in LNCaP and 22Rv1 cells. * $P < 0.05$, ** $P < 0.01$, *** $P < 0.001$ vs. sh-NC or vector, or as indicated. CASC11, cancer susceptibility candidate 11; NC, negative control; ns, not significant; OE-CASC11, CASC11 overexpression plasmid; RIP, RNA immunoprecipitation; sh, short hairpin.

YBX1 expression levels were validated via western blot when YBX1 was knocked down or overexpressed (Fig. S2). Colony formation and Transwell assays demonstrated that YBX1 knockdown significantly reversed the OE-CASC11-induced cell proliferation and migration of PCa cells (Fig. 7A-D). Furthermore, western blotting revealed that knockdown of YBX1 reversed the OE-CASC11-induced promotion of Cyclin A2, CDK2 and CDK4 protein expression (Fig. 7E), whereas the expression levels of p53 and p21 were returned to almost basal levels in response to YBX1 overexpression (Fig. 7F). These findings indicated that the CASC11/YBX1/p53 axis may exert role in PCa.

PBAE/si-CASC11 nanocomplexes inhibit the growth of PCa. The aforementioned results revealed that CASC11 may regulate the progression of PCa by interacting with the YBX1/p53 axis, thus highlighting the importance of CASC11 in the development of PCa. Nanoparticles encapsulating siRNA have emerged as promising small molecule inhibitor

substitutes. Because of its high transfection efficiency and low toxicity, PBAE is an ideal candidate for targeted delivery (21). As shown in Fig. S3A, CCK-8 results confirmed that PBAE exhibited no obvious toxicity when used at different concentrations in PCa cells. Therefore, PBAE was used as a carrier to deliver si-CASC11 and to suppress CASC11 expression. Nanocomplexes with varying proportions of PBAE and si-CASC11 were prepared based on their weight ratios. When the weight ratio of PBAE and si-CASC11 exceeded 40, relatively homogeneous nanoparticles formed. PBAE/si-CASC11 of 80:1 showed excellent performance with 2% si-CASC11 remaining, indicating a high loading efficiency of 98% (Fig. S3B). Additionally, both transmission electron microscopy and particle size potentiometer measurements indicated that the particle size of PBAE/si-CASC11 nanocomplexes was ~130 nm (Fig. S3C and D). Subsequently, subcutaneous xenograft tumor models were generated to further evaluate the efficacy of PBAE/si-CASC11 nanocomplexes on PCa progression *in vivo*. The knockdown efficiency of si-CASC11

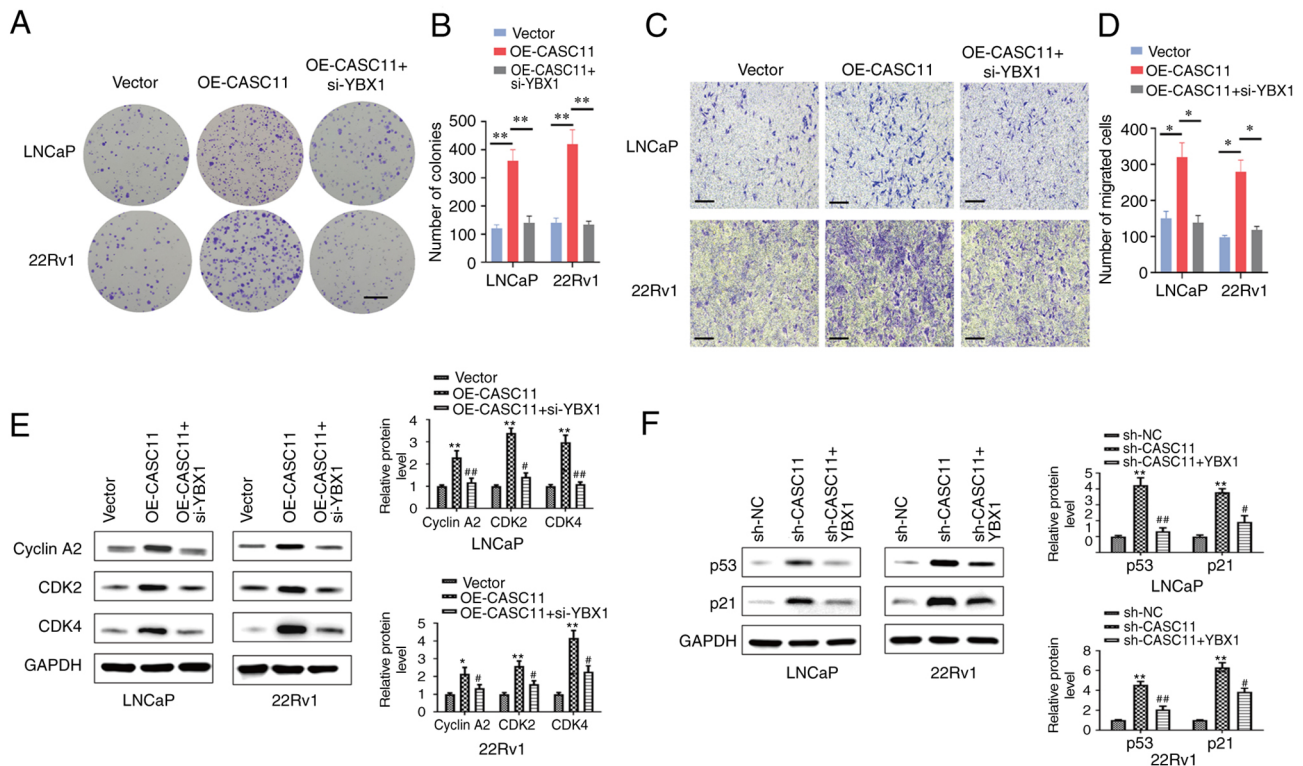


Figure 7. Knockdown of YBX1 in prostate cancer cells reverses the carcinogenic effects of CASC11. YBX1 knockdown reversed the OE-CASC11-induced (A and B) proliferation (scale bar, 500 μ m) and (C and D) migration (scale bar, 100 μ m) of LNCaP and 22Rv1 cells. * P <0.05, ** P <0.01. (E) Western blot analysis demonstrated that YBX1 knockdown abolished the OE-CASC11-induced promotion of Cyclin A2, CDK2 and CDK4 proteins. (F) Western blot analysis demonstrated that YBX1 overexpression reversed the sh-CASC11-induced increase in the expression levels of p21 and p53 proteins. * P <0.05, ** P <0.01 vs. the control group; # P <0.05, ## P <0.01 vs. the OE-CASC11 or sh-CASC11 group. CASC11, cancer susceptibility candidate 11; NC, negative control; OE-CASC11, CASC11 overexpression plasmid; sh, short hairpin; YBX1, Y-box binding protein 1.

in subcutaneous tumors was confirmed by RT-qPCR (Fig. S3E). The results revealed that the tumor size and weight of mice treated with PBAE/si-CASC11 nanocomplexes were significantly decreased compared with those treated with saline (Fig. 8A-C). Similarly, IHC revealed a substantial decrease in Ki-67 expression (Fig. 8D and E). H&E staining of the main organs, including the liver and kidney, further revealed that no notable morphological changes occurred in the groups, indicating a good biosecurity (Fig. S4). Therefore, PBAE/si-CASC11 nanocomplexes may be effective in suppressing PCa development and exhibited excellent therapeutic outcome on limiting tumor growth. A schematic diagram summarizing the findings of the present study is presented in Fig. 9.

Discussion

PCa is one of the major types of cancer affecting human health. Despite significant advances in therapeutic options, the mortality rate of PCa has not been markedly improved (22,23). Numerous studies have confirmed that lncRNAs serve vital roles in carcinogenesis. Dysregulation of lncRNAs have been reported to be strongly associated with tumor development; therefore, it is essential to understand the function and governing mechanisms of lncRNAs (24,25). Tumor-specific treatments may target certain lncRNAs and a number of lncRNA-associated molecular functions have been described in PCa, such as targeting other RNAs, activation of the

androgen receptor, and the modulation of epigenetic status through interactions with transcriptional regulators (26). The development of potentially effective alternative therapies for advanced PCa may be enhanced by targeting lncRNAs with cancer-specific expression patterns.

In the present study, the role of CASC11 in PCa was determined through TCGA and GEO dataset analyses, and was validated in PCa samples. The present results demonstrated that CASC11 was specifically upregulated in PCa tissues/cells and was implicated in cell cycle progression. The present study confirmed that CASC11 was closely associated with the progression of PCa and may be a potential therapeutic target for PCa.

Functionally, the present study assessed whether CASC11 was a key modulator of PCa tumorigenesis. Loss- and gain-of-function assays were conducted in two PCa cell lines, and the results of cell proliferation, colony formation and cell migration assays indicated the oncogenic properties of CASC11 in PCa cells. *In vivo* experiments further confirmed that knockdown of CASC11 could inhibit PCa progression. Hence, the present study demonstrated that CASC11 may exert oncogenic effects on PCa progression.

The cell cycle is a major regulatory mechanism for maintaining cellular physiological activity. Changes in different phases of the cell cycle are critical for cell proliferation, differentiation and senescence (27,28). Cell cycle progression analysis and western blotting revealed that CASC11 induced G₁/S transition and influenced the expression of cell cycle-related

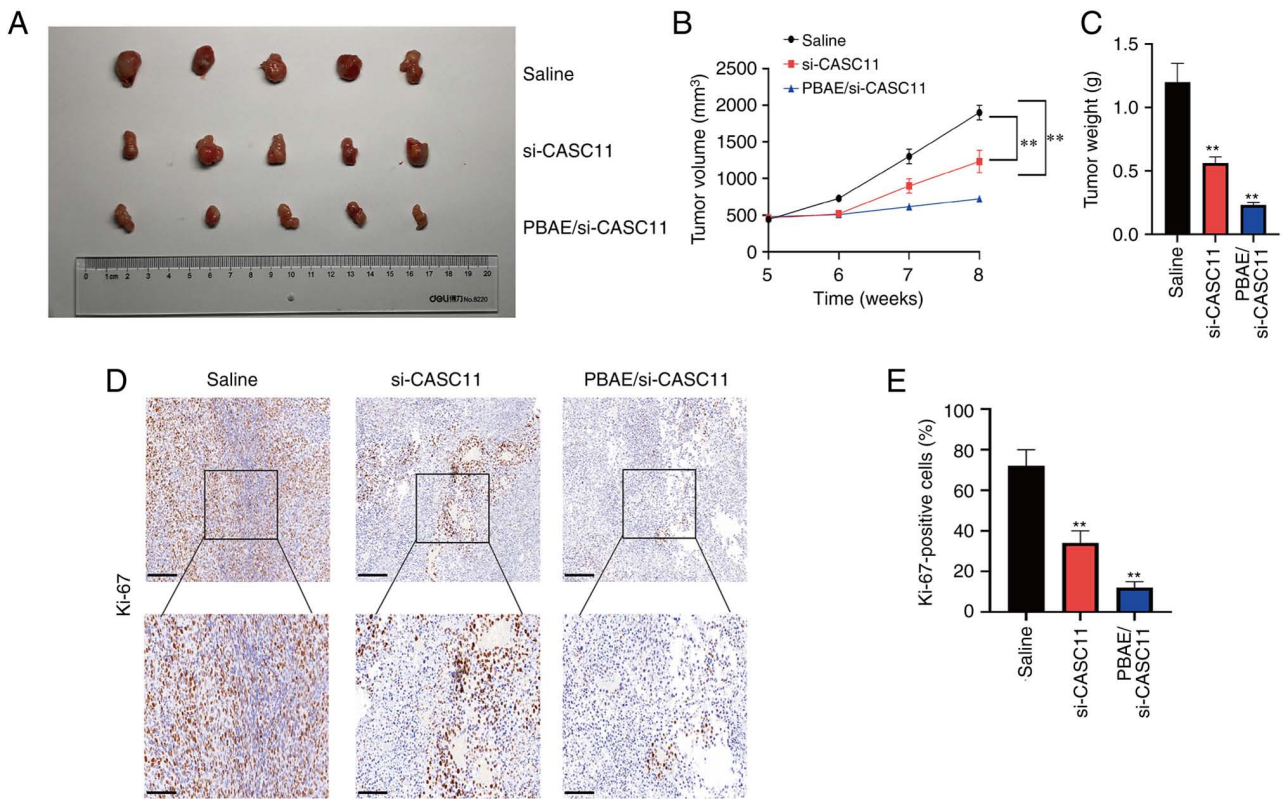


Figure 8. PBAE/si-CASC11 nanocomplexes may inhibit the progression of prostate cancer. (A-C) Weight and volume changes following 3 weeks of xenograft tumor treatment with saline, si-CASC11 or PBAE/si-CASC11. (D and E) Expression levels of Ki-67 were detected by immunohistochemistry. Scale bars, 100 and 200 μ m. **P<0.01 vs. saline group or as indicated. CASC11, cancer susceptibility candidate 11; PBAE, poly (β -amino ester); si, small interfering.

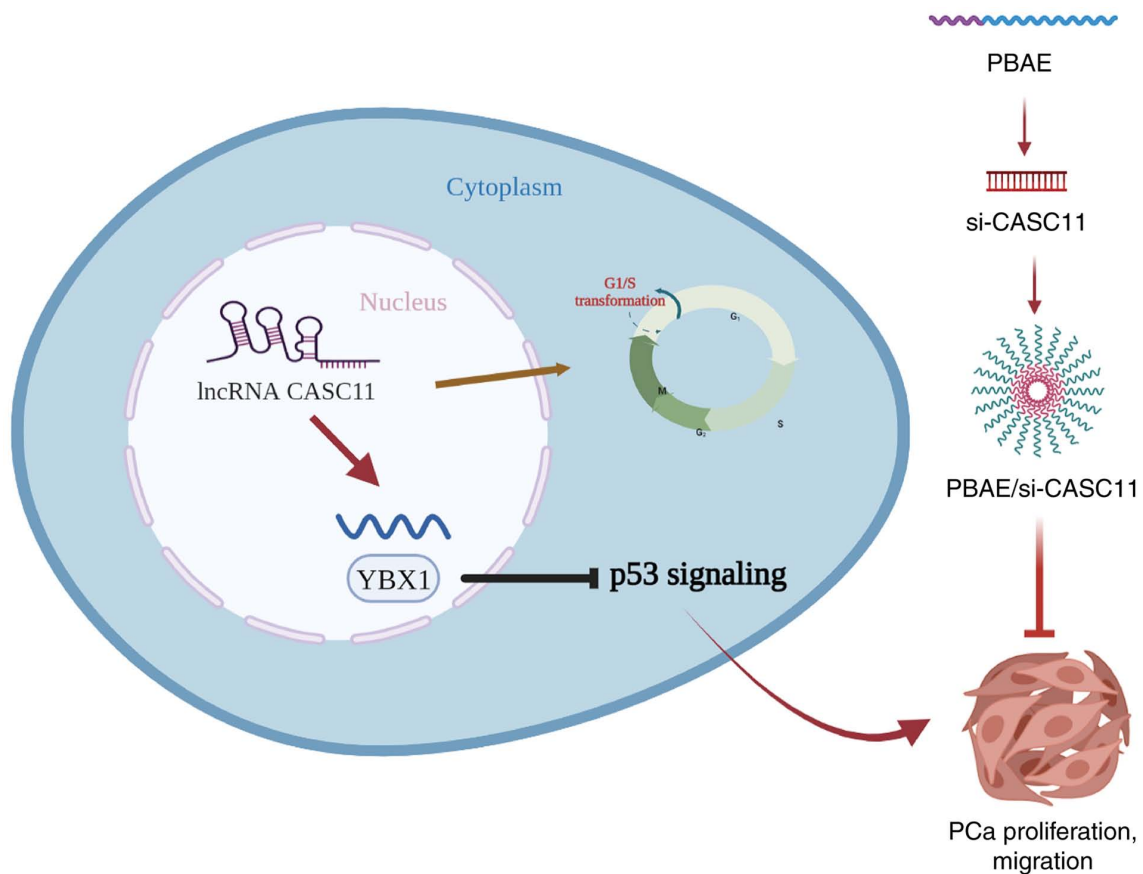


Figure 9. Schematic diagram summarizing the present study results. CASC11, cancer susceptibility candidate 11; lncRNA, long non-coding RNA; PBAE, poly (β -amino ester); PCa, prostate cancer; si, small interfering.

proteins. These findings indicated that CASC11 facilitated PCa cell proliferation by impacting cell cycle progression. As determined by RNA-seq and KEGG analyses between the sh-NC and sh-CASC groups, it was revealed that cell cycle signaling was the top enriched signaling pathway and it was suggested that the p53 signaling pathway may be involved in the molecular mechanism of CASC11. p53 functions as a tumor suppressor, triggering cell cycle arrest and apoptosis by stimulating downstream targets (29,30). It has been reported that several lncRNAs interact with the p53 signaling network, and serve as upstream regulators or downstream effectors of the apoptotic process (31). Mitra *et al* (32) previously reported that p53-responsive lncRNAs modulated the chemotherapy response through regulation of the nuclear p53 pathway. Chen *et al* (33) demonstrated that lncRNA RMRP promoted colorectal cancer cell growth by inactivating p53. In addition, a genome-wide transcriptome study previously reported that a pathway web containing 16 p53-targeted lncRNAs could form a strongly diagnostic tumor suppressor signature (34). Further analyses of expression levels in the present study confirmed that CASC11 caused inactivation of downstream p53 genes thus suggesting that the p53 gene may be regulated by CASC11.

Results from RNA pull-down and RIP assays identified an interaction between YBX1 and CASC11, which could mediate p53 transcriptional repression. YBX1 is a pivotal transcription factor that also serves as a multi-functional RNA-binding protein, which has been reported to be markedly overexpressed in a wide range of tumors (35). In addition, a number of cellular processes, along with tumor progression, have been shown to be mediated by YBX1 (36,37). In order to determine whether YBX1 affects cell progression and migration in PCa, a siRNA was used to silence the protein expression levels of YBX1. The experimental results indicated that suppressing YBX1 partially reversed CASC11-induced PCa progression and cell cycle-related protein expression. As a result, the present findings suggested that CASC11 may mediate PCa progression by interacting with YBX1. In addition, the upregulation of p53 caused by silencing CASC11 was reversed by YBX1 overexpression. These findings provide further evidence to support that CASC11/YBX1 binding may be critical to regulate p53 suppression.

The present study reported that CASC11 mediated the progression and migration of PCa by interacting with the YBX1/p53 axis, highlighting the critical role of CASC11 in the progression of PCa. Although evidence indicated that inhibition of CASC11 could reduce tumor proliferation, there are currently no small molecule inhibitors that target CASC11. High-throughput screening has been used to explore novel therapeutic candidates; however, some compounds have displayed less than encouraging results and the efficacy and specificity need to be improved (38,39). Therefore, extensive research into potent and specific CASC11 inhibitors is urgently required. Nanoparticles carrying siRNA have attracted attention as promising alternatives for cancer therapy (17,40,41). In the present study, a PBAE carrier was generated to deliver si-CASC11 and inhibit CASC11 expression. PBAE/si-CASC11 nanoparticles were revealed to be effective in blocking CASC11 expression and in enhancing the anti-tumor effects of CASC11 knockdown. The effectiveness and safety of PBAE/si-CASC11 nanoparticles need further clinical investigation.

In conclusion, the present study demonstrated that CASC11 was a valuable regulatory factor associated with the proliferation and migration of PCa cells. CASC11 contributed to PCa development and progression by interacting with YBX1 and suppressing p53 signaling. The present findings indicated that CASC11 may be a promising therapeutic target in PCa. Furthermore, PBAE/si-CASC11 nanocomplexes were generated, which may provide novel insights into the treatment of PCa.

Acknowledgements

Not applicable.

Funding

This work was supported by the National Natural Science Foundation of China (grant nos. 81972409 and 81672549).

Availability of data and materials

The sequencing data during the current study are not publicly available due to other unpublished research but are available from the corresponding author on reasonable request. Other data generated or analyzed during the current study are available from the corresponding author on reasonable request.

Authors' contributions

XS, WM and LY designed experiments. XS, SX and LY undertook statistical analyses. XS, YZ, LJ, XL, JZ, WM and BZ performed the experiments. XS, SX, and LY confirm the authenticity of all the raw data. XS, WM and YZ wrote the manuscript. All authors read and approved the final manuscript.

Ethics approval and consent to participate

Written informed consent was provided by the participants. The present study was approved by the Ethics Committee of The Second Affiliated Hospital of Anhui Medical University (approval no. 2021-130). The animal experiment was approved by the Animal Research Ethics Committee of The Second Affiliated Hospital of Anhui Medical University (approval no. 2021080).

Patient consent for publication

Not applicable.

Competing interests

The authors declare that they have no competing interests.

References

1. Siegel RL, Miller KD, Fuchs HE and Jemal A: Cancer statistics, 2022. *CA Cancer J Clin* 72: 7-33, 2022.
2. Marhold M, Kramer G, Krainer M and Le Magnen C: The prostate cancer landscape in Europe: Current challenges, future opportunities. *Cancer Lett* 526: 304-310, 2022.

3. Rebello RJ, Oing C, Knudsen KE, Loeb S, Johnson DC, Reiter RE, Gillissen S, Van der Kwast T and Bristow RG: Prostate cancer. *Nat Rev Dis Primers* 7: 9, 2021.
4. Zhu Y, Freedland SJ and Ye D: Prostate cancer and prostatic diseases best of asia, 2019: Challenges and opportunities. *Prostate Cancer Prostatic Dis* 23: 197-198, 2020.
5. Bridges MC, Daulagala AC and Kourtidis A: LNCcation: lncRNA localization and function. *J Cell Biol* 220: e202009045, 2021.
6. Lang C, Yin C, Lin K, Li Y, Yang Q, Wu Z, Du H, Ren D, Dai Y and Peng X: m(6)A modification of lncRNA PCAT6 promotes bone metastasis in prostate cancer through IGF2BP2-mediated IGF1R mRNA stabilization. *Clin Transl Med* 11: e426, 2021.
7. Wu G, Hao C, Qi X, Nie J, Zhou W, Huang J and He Q: LncRNA SNHG17 aggravated prostate cancer progression through regulating its homolog SNORA71B via a positive feedback loop. *Cell Death Dis* 11: 393, 2020.
8. Ghildiyal R, Sawant M, Renganathan A, Mahajan K, Kim EH, Luo J, Dang HX, Maher CA, Feng FY and Mahajan NP: Loss of long noncoding RNA NXTAR in prostate cancer augments androgen receptor expression and enzalutamide resistance. *Cancer Res* 82: 155-168, 2022.
9. Wang B, Xu W, Hu C, Liu K, Chen J, Guo C and Yuan C: Critical roles of the lncRNA CASC11 in tumor progression and cancer metastasis: The biomarker and therapeutic target potential. *Genes Dis* 9: 325-333, 2022.
10. Zhang Z, Zhou C, Chang Y, Zhang Z, Hu Y, Zhang F, Lu Y, Zheng L, Zhang W, Li X and Li X: Long non-coding RNA CASC11 interacts with hnRNP-K and activates the WNT/ β -catenin pathway to promote growth and metastasis in colorectal cancer. *Cancer Lett* 376: 62-73, 2016.
11. Song H, Liu Y, Li X, Chen S, Xie R, Chen D, Gao H, Wang G, Cai B and Yang X: Long noncoding RNA CASC11 promotes hepatocarcinogenesis and HCC progression through EIF4A3-mediated E2F1 activation. *Clin Transl Med* 10: e220, 2020.
12. Cheng N, Wu J, Yin M, Xu J, Wang Y, Chen X, Nie Z and Yin J: LncRNA CASC11 promotes cancer cell proliferation in hepatocellular carcinoma by inhibiting miRNA-188-5p. *Biosci Rep*: Apr 30, 2019 (Epub ahead of print).
13. Cui Y, Shen G, Zhou D and Wu F: CASC11 overexpression predicts poor prognosis and regulates cell proliferation and apoptosis in ovarian carcinoma. *Cancer Manag Res* 12: 523-529, 2020.
14. Capik O, Sanli F, Kurt A, Ceylan O, Suer I, Kaya M, Ittmann M and Karatas OF: CASC11 promotes aggressiveness of prostate cancer cells through miR-145/IGF1R axis. *Prostate Cancer Prostatic Dis* 24: 891-902, 2021.
15. Humphrey PA, Moch H, Cubilla AL, Ulbright TM and Reuter VE: The 2016 WHO classification of tumours of the urinary system and male genital organs-part b: Prostate and bladder tumours. *Eur Urol* 70: 106-119, 2016.
16. Livak KJ and Schmittgen TD: Analysis of relative gene expression data using real-time quantitative PCR and the 2(-Delta Delta C(T)) method. *Methods* 25: 402-408, 2001.
17. Mao W, Wang K, Xu B, Zhang H, Sun S, Hu Q, Zhang L, Liu C, Chen S, Wu J, *et al*: ciRS-7 is a prognostic biomarker and potential gene therapy target for renal cell carcinoma. *Mol Cancer* 20: 142, 2021.
18. Yan X, Pan Q, Xin H, Chen Y and Ping Y: Genome-editing prodrug: Targeted delivery and conditional stabilization of CRISPR-Cas9 for precision therapy of inflammatory disease. *Sci Adv* 7: eabj0624, 2021.
19. Mortensen MM, Høyer S, Lynnerup AS, Ørntoft TF, Sørensen KD, Borre M and Dyrskjød L: Expression profiling of prostate cancer tissue delineates genes associated with recurrence after prostatectomy. *Sci Rep* 5: 16018, 2015.
20. Arredouani MS, Lu B, Bhasin M, Eljanne M, Yue W, Mosquera JM, Bubley GJ, Li V, Rubin MA, Libermann TA and Sanda MG: Identification of the transcription factor single-minded homologue 2 as a potential biomarker and immunotherapy target in prostate cancer. *Clin Cancer Res* 15: 5794-5802, 2009.
21. Yang C, Xue Z, Liu Y, Xiao J, Chen J, Zhang L, Guo J and Lin W: Delivery of anticancer drug using pH-sensitive micelles from triblock copolymer MPEG-b-PBAE-b-PLA. *Mater Sci Eng C Mater Biol Appl* 84: 254-262, 2018.
22. Yamada Y and Beltran H: The treatment landscape of metastatic prostate cancer. *Cancer Lett* 519: 20-29, 2021.
23. Adamaki M and Zoumpourlis V: Prostate cancer biomarkers: From diagnosis to prognosis and precision-guided therapeutics. *Pharmacol Ther* 228: 107932, 2021.
24. Hua JT, Chen S and He HH: Landscape of noncoding RNA in prostate cancer. *Trends Genet* 35: 840-851, 2019.
25. Tan YT, Lin JF, Li T, Li JJ, Xu RH and Ju HQ: LncRNA-mediated posttranslational modifications and reprogramming of energy metabolism in cancer. *Cancer Commun (Lond)* 41: 109-120, 2021.
26. Xu YH, Deng JL, Wang G and Zhu YS: Long non-coding RNAs in prostate cancer: Functional roles and clinical implications. *Cancer Lett* 464: 37-55, 2019.
27. Ahmad I, Fakhri S, Khan H, Jeandet P, Aschner M and Yu ZL: Targeting cell cycle by β -carboline alkaloids in vitro: Novel therapeutic prospects for the treatment of cancer. *Chem Biol Interact* 330: 109229, 2020.
28. Dyshlovoy SA, Tarbeeva D, Fedoreyev S, Busenbender T, Kaune M, Veselova M, Kalinovskiy A, Hauschild J, Grigorochuk V, Kim N, *et al*: Polyphenolic compounds from lespedeza bicolor root bark inhibit progression of human prostate cancer cells via induction of apoptosis and cell cycle arrest. *Biomolecules* 10: 451, 2020.
29. Duffy MJ, Synnott NC, O'Grady S and Crown J: Targeting p53 for the treatment of cancer. *Semin Cancer Biol* 79: 58-67, 2022.
30. Kim MP, Li X, Deng J, Zhang Y, Dai B, Allton KL, Hughes TG, Siangco C, Augustine JJ, Kang Y, *et al*: Oncogenic KRAS recruits an expansive transcriptional network through mutant p53 to drive pancreatic cancer metastasis. *Cancer Discov* 11: 2094-2111, 2021.
31. Zhang A, Xu M and Mo YY: Role of the lncRNA-p53 regulatory network in cancer. *J Mol Cell Biol* 6: 181-191, 2014.
32. Mitra S, Muralidharan SV, Di Marco M, Juvvuna PK, Kosalai ST, Reischl S, Jachimowicz D, Subhash S, Raimondi I, Kurian L, *et al*: Subcellular distribution of p53 by the p53-responsive lncRNA NBAT1 determines chemotherapeutic response in neuroblastoma. *Cancer Res* 81: 1457-1471, 2021.
33. Chen Y, Hao Q, Wang S, Cao M, Huang Y, Weng X, Wang J, Zhang Z, He X, Lu H and Zhou X: Inactivation of the tumor suppressor p53 by long noncoding RNA RMRP. *Proc Natl Acad Sci USA* 118: e2026813118, 2021.
34. Sanchez Y, Segura V, Marin-Bejar O, Athie A, Marchese FP, Gonzalez J, Bujanda L, Guo S, Matheu A and Huarte M: Genome-wide analysis of the human p53 transcriptional network unveils a lncRNA tumour suppressor signature. *Nat Commun* 5: 5812, 2014.
35. Lyabin DN, Eliseeva IA and Ovchinnikov LP: YB-1 protein: Functions and regulation. *Wiley Interdiscip Rev RNA* 5: 95-110, 2014.
36. Gandhi M, Groß M, Holler JM, Coggins SA, Patil N, Leupold JH, Munschauer M, Schenone M, Hartigan CR, Allgayer H, *et al*: The lncRNA lincNMR regulates nucleotide metabolism via a YBX1-RRM2 axis in cancer. *Nat Commun* 11: 3214, 2020.
37. Zheng X, Zhang J, Fang T, Wang X, Wang S, Ma Z, Xu Y, Han C, Sun M, Xu L, *et al*: The long non-coding RNA PIK3CD-AS2 promotes lung adenocarcinoma progression via YBX1-mediated suppression of p53 pathway. *Oncogenesis* 9: 34, 2020.
38. Itsumi M, Shiota M, Sekino Y, Ushijima M, Kashiwagi E, Takeuchi A, Inokuchi J, Kajioka S, Uchiumi T and Eto M: High-throughput screen identifies 5-HT receptor as a modulator of AR and a therapeutic target for prostate cancer. *Prostate* 80: 885-894, 2020.
39. Adams J, Casali A and Campbell K: Sensitive high-throughput assays for tumour burden reveal the response of a drosophila melanogaster model of colorectal cancer to standard chemotherapies. *Int J Mol Sci* 22: 5101, 2021.
40. Yari H, Gali H and Awasthi V: Nanoparticles for targeting of prostate cancer. *Curr Pharm Des* 26: 5393-5413, 2020.
41. Mezghrani B, Ali LMA, Richeter S, Durand JO, Hesemann P and Bettache N: Periodic mesoporous ionosilica nanoparticles for green light photodynamic therapy and photochemical internalization of siRNA. *ACS Appl Mater Interfaces* 13: 29325-29339, 2021.

